Study of neutron and proton distributions in Ca, Sn, and Ba isotopes by polarized electron scattering

Toshio Suzuki
Department of Physics, College of Humanities and Sciences, Nihon University, Sakurajosui 3-25-40, Setagaya-ku, Tokyo 156, Japan
(Received 5 July 1994)

Asymmetries of elastic electron scattering at low momentum transfer ($q \leq 1$ fm^{-1}) are used to study the difference of radii between neutron and proton distributions in nuclei such as Ca, Sn, and Ba isotopes. The asymmetry is shown to be another powerful tool to study the difference of neutron and proton distributions in nuclei.

PACS number(s): 21.10.Gv, 21.60.Jz, 24.70.+s, 25.30.Bf

I. INTRODUCTION

Recently, much work has been devoted to the strange quark content of the nucleon [1–5]. It has been shown [6,7] that the asymmetry of longitudinally polarized electron scattering in nuclear isoscalar magnetic transitions, for example, ^{12}C$(\vec{e},e')^{12}$C$(1^+,$ 12.71 MeV) and ^{2}H$(\vec{e},e)^2$H, is quite sensitive to the vector current type strange quark matrix element of the nucleon, $\langle N|\bar{s}\gamma_\mu s|N\rangle$. Cross sections of ν scattering in isoscalar magnetic transitions are found to be sensitive to the axial vector current strange quark matrix element of the nucleon, $\langle N|\bar{s}\gamma_\mu\gamma^5 s|N\rangle$; for example, ^{12}C$(\nu,\nu')^{12}C(1^+,$ 12.71 MeV) and ^{10}B$(\nu,\nu')^{10}$B$(2^+, T=0,$ 3.59 MeV) [8].

Asymmetries of unpolarized electrons from polarized nuclear targets have also been investigated in deuterium [7], and their sensitivities to $\langle N|\bar{s}\gamma_\mu s|N\rangle$ and $\langle N|\bar{s}\gamma_\mu\gamma^5 s|N\rangle$ have been found to depend on the direction of the polarization of the target.

The actual observation of these effects, however, is not easy in polarized electron scattering because of the smallness of the cross sections of magnetic transitions as well as their asymmetries, which are of the order of 10^{-5}. Experiments are feasible for ^{1}H$(\vec{e},e)^1$H [9] and within the accessible range for $^2\vec{\text{H}}(e,e)^2$H or ^{2}H$(\vec{e},e)^2$H. The ν scattering experiments are, in principle, accessible. A comprehensive review of the present status and future prospects of semileptonic neutral current studies is given in Ref. [10].

In a previous work [11], we therefore considered asymmetries of polarized elastic Coulomb electron scattering which is experimentally more feasible due to its large cross section. We found that in ^{208}Pb$(\vec{e},e)^{208}$Pb, at low momentum transfer ($q \leq 1.5$ fm^{-1}), the effects of the strangeness vector form factors of the nucleon on the asymmetry are smaller than those caused by the difference of neutron and proton distributions in nuclei. The measurement of the asymmetry at low q can give us accurate information on the difference of the radii between neutron and proton distributions. Investigations with simple wave functions have been done for some closed-shell nuclei [12].

In the present paper, we extend our previous investigation to other nuclei such as Ca, Sn, and Ba isotopes and study the sensitivity of the asymmetries to the difference of neutron and proton distributions. Especially, we are interested in the mass number dependence of the difference in each kind of isotope.

II. ASYMMETRIES OF POLARIZED ELECTRON SCATTERING

A. Asymmetries in the low q region

Here we summarize some formulas for the asymmetry of polarized elastic electron scattering and clarify what we can learn from its measurement in the low momentum transfer region. The parity-violating asymmetry for longitudinally polarized electron Coulomb scattering from a target with spin 0 is defined by $A = (d\sigma\uparrow - d\sigma\downarrow)/(d\sigma\uparrow + d\sigma\downarrow)$, where $d\sigma\uparrow$ ($d\sigma\downarrow$) is the cross section for the right- (left-) handed polarized electron, and can be expressed as

$$A = -\frac{Gq_\mu^2}{2\pi\alpha\sqrt{2}}\Big\{(G_E^{\rm IV} - 2\sin^2\theta_W G_E^P - \tfrac{1}{2}G_E^S)\langle 0^+||\sum_p j_0 Y_0||0^+\rangle + (-G_E^{\rm IV} - 2\sin^2\theta_W G_E^n - \tfrac{1}{2}G_E^S)$$
$$\times\langle 0^+||\sum_n j_0 Y_0||0^+\rangle\Big\}\Big/\Big\{G_E^P\langle 0^+||\sum_p j_0 Y_0||0^+\rangle + G_E^n\langle 0^+||\sum_n j_0 Y_0||0^+\rangle\Big\}\,. \quad (1)$$

Here, G_E^P (G_E^n) is the electric form factor of the proton (neutron) with the relativistic Darwin-Foldy correction term [13], G_E^S is the strangeness form factor of the nucleon, and $G_E^{\rm IV} = \frac{1}{2}(G_E^P - G_E^n)$ is the isovector electric form factor of the nucleon. $q_\mu^2 = q^2 - q_0^2$ with q the effective momentum transfer and q_0 the energy transfer which vanishes for the elastic scattering, $\alpha \simeq \frac{1}{137}$ is the fine-structure constant, and $G \simeq 10^{-5}/m^2$ (where m is

the mass of the proton) is the weak coupling constant. In actual calculations, contributions from spin-orbit current densities are included [13].

When N (neutron number)=Z (proton number) and the neutron and proton distributions are the same, the asymmetry is given by

$$A = \frac{Gq_\mu^2}{2\pi\alpha\sqrt{2}} 2\sin^2\theta_W \left(1 + \frac{G_E^S}{2(G_E^P + G_E^n)\sin^2\theta_W}\right) . \quad (2)$$

The dominant term is determined by the value of the Weinberg angle θ_W [14,15], and there is a small correction from G_E^S. A deviation of the asymmetry from Eq. (2) reflects the difference between the neutron and proton distributions in nuclei. In the next subsection, we will show the calculated values of

$$A_S = \pi\alpha\sqrt{2}A/(Gq_\mu^2\sin^2\theta_W) \quad (3)$$

and discuss its deviations from unity for ^{40}Ca$(\vec{e},e)^{40}$Ca.

When $N > Z$ and if we can neglect G_E^n and G_E^S compared to G_E^P, the asymmetry can be expressed as

$$A = -\frac{Gq_\mu^2}{4\pi\alpha\sqrt{2}}\Big\{(1-4\sin^2 q_W)\langle 0^+||\sum_p j_0 Y_0||0^+\rangle - \langle 0^+||\sum_n j_0 Y_0||0^+\rangle\Big\} \times \Big(\langle 0^+||\sum_p j_0 Y_0||0^+\rangle\Big)^{-1} , \quad (4)$$

that is,

$$A_S = \frac{1}{4\sin^2\theta_w}\frac{N}{Z}\left(1 - (1-4\sin^2\theta_W)\frac{Z}{N} + \frac{\langle 0^+||\sum_n j_0 Y_0||0^+\rangle/N - \langle 0^+||\sum_p j_0 Y_0||0^+\rangle/Z}{\langle 0^+||\sum_p j_0 Y_0||0^+\rangle/Z}\right) . \quad (5)$$

Since the value of $1 - 4\sin^2\theta_W$ is as small as 0.08, the asymmetry in the low q region is determined by the ratio of the neutron distribution to the proton distribution. At $q = 0$,

$$A_S = A_S^0 \equiv \frac{1}{4\sin^2\theta_W}\left\{\frac{N}{Z} - (1-4\sin^2\theta_W)\right\} . \quad (6)$$

The deviation of A_S from the value A_S^0 at low q can be expressed in terms of the difference between the squared radii of neutron and proton distributions, $\Delta r_{np}^2 = \langle r_n^2\rangle - \langle r_p^2\rangle$. When the approximation $j_0(qr) = 1 - \frac{1}{6}q^2r^2$ is valid, we obtain

$$A_S \approx \frac{1}{4\sin^2\theta_W}\frac{N}{Z}\left\{1 - (1-4\sin^2\theta_W)\frac{Z}{N} - \frac{q^2}{6}(\langle r_n^2\rangle - \langle r_p^2\rangle)\right\} = A_S^0 - \frac{1}{4\sin^2\theta_W}\frac{N}{Z}\frac{q^2}{6}(\langle r_n^2\rangle - \langle r_p^2\rangle) . \quad (7)$$

Thus, A_S becomes larger (smaller) than A_S^0 when $\langle r_n^2\rangle$ is smaller (larger) than $\langle r_p^2\rangle$.

B. Ca isotopes

We first discuss the Ca isotopes. In this case, Hartree-Fock (HF) calculations give larger differences between radii of neutron and proton distributions (Δr_{np}) than experiments [16] as the mass number (A) approaches $A = 48$. In other words, the experimental Δr_{np} does not increase with the number of excess neutrons, while the HF result increases monotonically as the number of excess neurons increases. We investigate how these differences between experiments and HF calculations affect the asymmetries of polarized electron scattering in the low momentum transfer region.

The effects of the difference between the neutron and proton distributions in ^{40}Ca, ^{42}Ca, ^{44}Ca, and ^{48}Ca on A_S are shown in Fig. 1. G_E^S is fixed to be zero. The curves with $A_S = 1.0$, 1.109, 1.217, and 1.435 at $q = 0$ [see Eq. (6)] correspond to ^{40}Ca, ^{42}Ca, ^{44}Ca, and ^{48}Ca, respectively. Three different HF wave functions are used. The results obtained with the use of SGII-HF wave functions [17] and those of Tondeur (HF-T) [18] are shown by the solid and dashed curves, respectively. The HF-T wave functions are constructed so as to reproduce the experimental charge radii r_c and density distributions of closed-shell nuclei as well as possible. r_c obtained by HF-T changes little as A increases from 40 to 48. The dotted curve is obtained by using the wave functions of Tondeur modified such as to reproduce the experimental values of $r_n = \sqrt{\langle r_n^2\rangle}$ and $r_p = \sqrt{\langle r_p^2\rangle}$. The nucleon form factors given by Galster *et al.* [19] are used. The deviation of A_S from A_S^0 shows the effect of the difference between neutron distributions and proton distributions. A_S gradually departs from A_S^0 as q increases. The values of $\Delta r_{np}^2 = \langle r_n^2\rangle - \langle r_p^2\rangle$ for the isotopes are tabulated in Table I. The quoted experimental values are determined by $\pi^\pm$ scattering [20]. With increasing q, A_S decreases

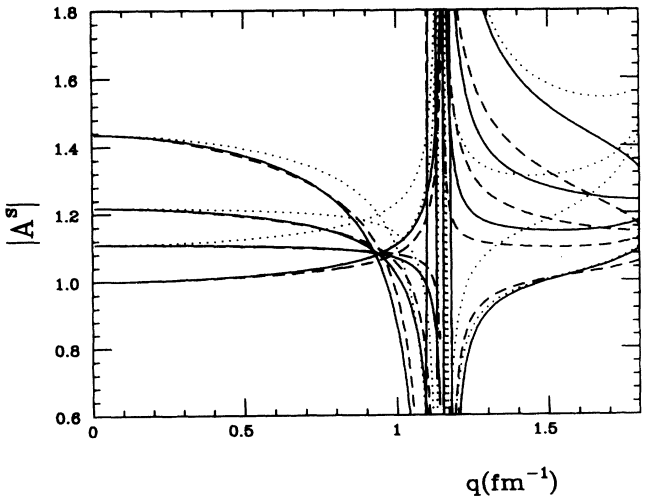

FIG. 1. Calculated asymmetries for Ca isotopes. Solid and dashed curves are obtained by using the SGII-HF and HF-T wave functions, respectively. The dotted curve is obtained by using the modified HF-T wave functions which reproduce the experimental values of r_n and r_p.

TABLE I. Calculated and experimental rms charge-neutron, and proton radii (r_c, r_n, and r_p, respectively, in fm) of Ca isotopes. Those calculated with the use of the SGII (Tondeur's) HF wave functions are denoted by SGII (Ton). Exp refers to the experimental values, $\Delta r^2_{np} = r^2_n - r^2_p$ (in fm^2).

A	40	42	44	46	48
SGII					
r_c	3.44	3.45	3.46	3.46	3.47
r_n	3.27	3.36	3.44	3.51	3.57
r_p	3.32	3.35	3.37	3.39	3.41
Δr^2_{np}	−0.330	0.067	0.477	0.828	1.117
Ton					
r_c	3.47	3.47	3.47	3.47	3.48
r_n	3.32	3.39	3.50	3.60	3.68
r_p	3.36	3.37	3.36	3.36	3.37
Δr^2_{np}	−0.267	0.135	0.960	1.670	2.186
Exp					
r_c	3.45	3.48	3.49	3.47	3.45
r_n	3.31	3.33	3.42		3.43
r_p	3.36	3.37	3.39		3.32
Δr^2_{np}	−0.334	−0.268	0.204		0.743

from A^0_S for positive Δr^2_{np} and increases from A^0_S for negative Δr^2_{np}. Note that for ^{42}Ca the dotted curve bends in the direction opposite to the solid and dashed curves. In the case of ^{40}Ca, the difference between the HF results and the experimental values for Δr^2_{np} is as small as 0.004–0.067 fm^2. It increases as the mass number increases: 0.068–0.335 fm^2 for ^{42}Ca, 0.273–0.756 fm^2 for ^{44}Ca, and 0.374–1.443 fm^2 for ^{48}Ca. Hence a discrimination between wave functions becomes possible for the cases of ^{42}Ca, ^{44}Ca, and ^{48}Ca.

The effects of G^S_E on the asymmetry are shown in Fig. 2 for ^{40}Ca and ^{48}Ca. The SGII-HF wave functions are used. The solid curve is obtained with $G^S_E = 0$. Three kinds of G^S_E are used. The dashed curve shows the calculated result obtained with the Galster's parametrization: $G^S_E = \rho_S \tau (1 + \lambda^V_D \tau)^{-2}(1 + \lambda^S_E \tau)^{-1}$ with $\tau = q^2_\mu/4m^2$ and $\rho_S = -\frac{2}{3}m^2 r^2_S - F^S_2(0)$. Here $F^S_2(0)$ is the strange anomalous magnetic moment of the nucleon and r_S is the strangeness radius defined by $r^2_S = -6dF^S_1(0)/dq^2$. The parameters $\rho_S = 2$, $\lambda^V_D = 4.97$, and $\lambda^S_E = 5.6$ [21] are employed. The three-pole form of F^S_1 and $F^S_2 (G^S_E = F^S_1 + \tau F^S_2)$ given by Jaffe [22] is used for the dash-dotted curve. The parameter set of Ref. [22] which gives $F^S_2(0) = -0.25$ and $r^2_S = 0.11$ fm^2 ($\rho_S = -1.91$) is used. The dotted curve is obtained with a four-pole form with asymptotic $(q^2)^{-2}$ falloff for F^S_1 and $(q^2)^{-3}$ falloff for F^S_2. This form factor with the 4th pole at 1.8 GeV gives $F^S_2(0) = -0.16$ and $r^2_S = 0.06$ fm^2 ($\rho_S = -1.06$) [11]. This form factor is considered to be closest to the reality. Positive (negative) values of ρ_S enhance (suppress) A_S at finite q. For ^{40}Ca, G^S_E affects A_S by $-0.9 - 1.2\%$ at $q = 0.5$ fm^{-1}, $-1.7 - 2.3\%$ at $q = 0.7$ fm^{-1}, and $-3.7 - 4.7\%$ at $q = 1$ fm^{-1}. These deviations are comparable to those caused by Δr^2_{np} in the case of ^{40}Ca. It is, therefore, not easy to discriminate and identify the effects of G^S_E and (or) Δr^2_{np} in ^{40}Ca at low q. In the case of ^{48}Ca, A_S is affected by G^S_E by $-0.7 - 1.0\%$ at $q = 0.5$ fm^{-1}, $-1.4 - 2.0\%$, at $q = 0.7$ fm^{-1}, and $-4.0 - 4.8\%$ at $q = 1$ fm^{-1}. These effects are smaller than those caused by Δr^2_{np}. It is, thus, possible to discriminate the effects of Δr^2_{np} from those of G^S_E in ^{48}Ca. The effects of G^S_E on A_S are similar also for the other Ca isotopes as they are determined by the difference in r^2_S: $\Delta r^2_S = 0.05 - 0.18$ fm^2.

We can conclude from the above that, in spite of some ambiguities due to the effects of G^S_E, by looking at A_S we can distinguish the isotope dependence of Δr^2_{np} obtained by HF calculations from the experimental Δr^2_{np} determined from π-nucleus scattering. The measurement of the asymmetry at low q can, thus, be another useful tool

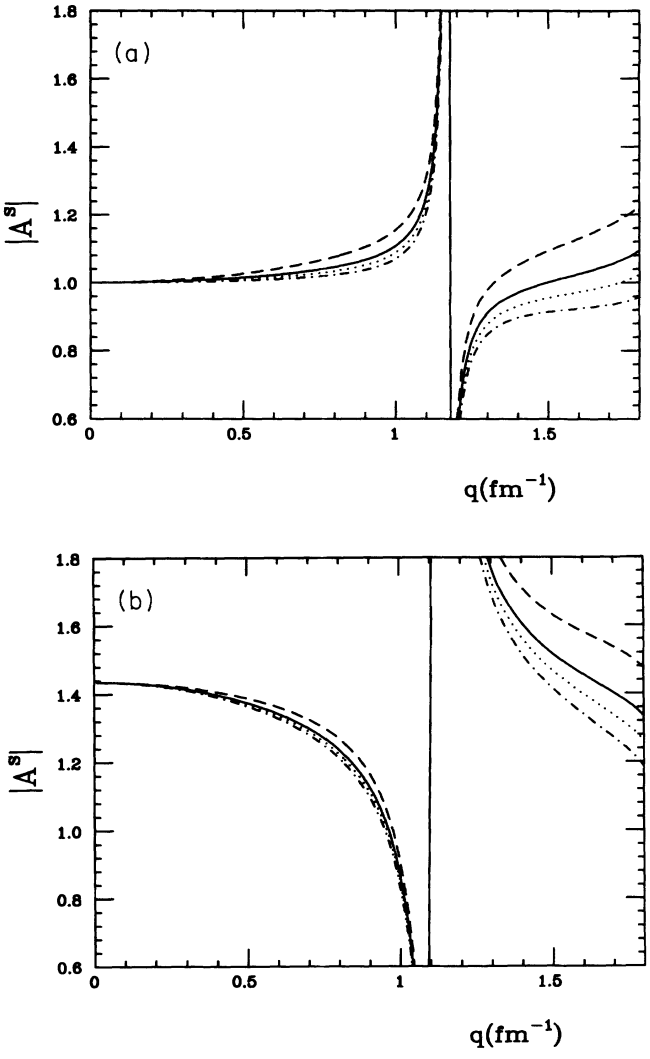

FIG. 2. (a) Calculated asymmetries for ^{40}Ca obtained with the use of SGII-HF wave functions. The solid curve is obtained with $G^S_E = 0$. The dashed one is calculated with G^S_E of dipole form given by Galster *et al.* [19]. The dash-dotted (dotted) curve is obtained with G^S_E of three-pole (four-pole) form. (b) The same as in (a) for ^{48}Ca.

to obtain the isotope dependence of Δr_{np}^2, though its actual measurement is not easy for Ca isotopes at present. In the case of $A = 48$, whose first excited state is at 3.8 MeV, the energy resolution required is looser than in the case of ^{208}Pb where the first excited state is at 2.6 MeV, but the magnitude of the cross section is smaller by a factor $(20/82)^2$. Therefore, in order to determine Δr_{np} to the accuracy of 1%, the machine time required is about 10 times that required for the case of ^{208}Pb, that is, ~ 30 days$/P^2$ at $q = 0.5$ fm^{-1} where P is the polarization of the electron, under the same experimental conditions as in Ref. [12]. We hope that a better experimental situation than the present level can be acquired in the near future.

C. Sn isotopes

Next we discuss the Sn isotopes. The experimental charge radii of Sn isotopes change almost linearly as N increases from 60 to 75 [16]. The difference of radii between neutron and proton distributions, Δr_{np}, can be obtained from an analysis of medium-energy proton nucleus scattering [23]. The deduced values for $\Delta r_{np}/r_0$, where $r_0 = (r_p + r_n)/2$, are $(3.2 \pm 1.1)\%$ and $(5.3 \pm 2.4)\%$ for ^{116}Sn and ^{124}Sn, respectively. The analysis of a recent measurement of the cross section of the isovector giant dipole resonance (GDR) excited by inelastic α scattering, ^{116,124}Sn$(\alpha, \alpha'\gamma_0)$, gives $0.7^{+2.3}_{-0.7}\%$ and $4.1^{+2.1}_{-2.5}\%$ for $\Delta r_{np}/r_0$ in the case of ^{116}Sn and ^{124}Sn, respectively [24]. Here, we investigate the sensitivity of the asymmetry of polarized electron scattering at low q to Δr_{np} in the Sn isotopes.

We compare the calculated asymmetries of elastic electron scattering from ^{116}Sn, ^{120}Sn, and ^{124}Sn. The calculated results obtained by using the HF-SGII wave functions are shown by the solid curves in Fig. 3. Effects of the pairing force are taken into account by the constant-gap approach $\Delta = 11.2/A^{1/2}$ MeV [25] throughout the present investigation. The values of A_S at $q = 0$ (A_S^0) for ^{116}Sn, ^{120}Sn, and ^{124}Sn are 1.348, 1.435, and 1.522, respectively. The values of r_n, r_p, $\Delta r_{np}^2 = r_n^2 - r_p^2$, and $\Delta r_{np}/r_0$ for the HF-SGII wave functions as well as for the other two wave functions are shown in Table II. As the Δr_{np}^2 are positive, A_S decreases from A_S^0 as q increases. The calculated results obtained by using the modified HF-SGII wave functions are shown in Fig. 3 by the dotted curves. In this case, the values of r_n for ^{116}Sn and ^{124}Sn are constrained to reproduce the observed values of $\Delta r_{np}/r_0$, 0.7% for ^{116}Sn and 4.1% for ^{124}Sn. The values of Δr_{np}^2 are modified to 0.292 and 1.79 fm^2 for ^{116}Sn, respectively (see Table II). As the value of Δr_{np}^2 is decreased (increased), A_S decreases more slowly (rapidly) for ^{116}Sn (^{124}Sn) compared to the case for HF-SGII. The dotted curves can be considered to represent the experimental asymmetries, which correspond to the values of Δr_{np}^2 obtained from $(\alpha, \alpha'\gamma)$ reactions. The dashed curves in Fig. 3 show the calculated results obtained by using the HF wave functions of Tondeur (HF-T) [18]. Among the three isotopes, the decrease of A_S is most rapid for ^{116}Sn, as the value of Δr_{np}^2 is largest as shown in Table II. The decrease of A_S for ^{124}Sn is similar to the case of the modified HF-SGII. We can distinguish the results obtained by the three HF wave functions for the isotope dependence of A_S at low q. As the Δr_{np}^2 for the HF-T case are close to the experimental values obtained from proton scattering, the dashed curves can be considered to be close to the experimental asymmetries. We have, thus, a chance to distinguish further between

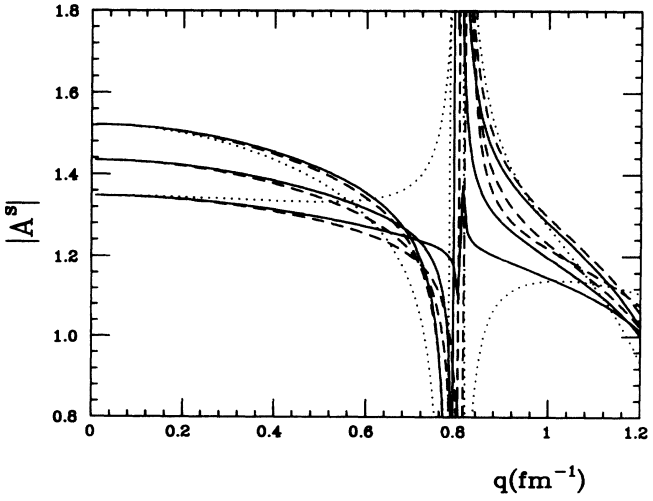

FIG. 3. The same as in Fig. 1 for Sn isotopes. The solid and dashed curves are the same as in Fig. 1. The dotted curve is obtained by using the modified SGII-HF wave functions which reproduce the observed values of $\Delta r_{np}/r_0$.

TABLE II. The same as in Table I for Sn isotopes. $\Delta r_{np} = r_n - r_p$ and $r_0 = (r_n + r_p)/2$. SGII^m means that r_n is modified to reproduce experimental values of $\Delta r_{np}/r_0$ obtained from $(\alpha, \alpha'\gamma)$ reaction.

A	116	120	124
SGII			
r_c	4.26	4.65	4.68
r_n	4.36	4.70	4.76
r_p	4.55	4.58	4.61
Δr_{np}^2	0.734	1.11	1.41
$\Delta r_{np}/r_0$	1.7%	2.6%	3.2%
SGII^m			
r_n	4.58	4.70	4.80
Δr_{np}^2	0.292	1.11	1.79
$\Delta r_{np}/r_0$	0.7%	2.6%	4.1%
Ton			
r_c	4.55	4.59	4.63
r_n	4.62	4.71	4.76
r_p	4.47	4.50	4.56
Δr_{np}^2	1.36	1.93	1.86
$\Delta r_{np}/r_0$	3.3%	4.6%	4.3%
Exp			
$\Delta r_{np}/r_0$			
$(\alpha, \alpha'\gamma)$	$0.7^{+2.3}_{-0.7}\%$		$4.1^{+2.1}_{-2.5}\%$
(p, p)	(3.2±1.1)%		(5.3±2.4)%

the two sets of observed values of Δr_{np}^2, if the experimental uncertainties can be reduced.

We have better experimental feasibility for Sn isotopes than for Ca isotopes, though the feasibility is less than in the case of ^{208}Pb. Energy resolution required for the Sn isotopes is about twice that required for ^{208}Pb, and the magnitudes of the cross sections are smaller by a factor $(50/82)^2$. The machine time required to discern Δr_{np} to the accuracy of 1% becomes several times that required for ^{208}Pb, which seems within the reach of the present experimental situation. The determination of Δr_{np} to the accuracy of 1% is better than (or comparable to) the accuracy of $(\alpha, \alpha'\gamma)$ and (p,p) experiments. If we allow for an accuracy of 2%, which is comparable to those in the $(\alpha, \alpha'\gamma)$ and (p,p) experiments, the measurement of the asymmetries is feasible already. If one can actually measure the asymmetries for the Sn isotopes, we have another powerful tool to determine the difference in radii of neutron and proton distributions.

D. Ba isotopes

In this subsection we discuss the Ba isotopes. Experimentally, the isotope dependence of the charge radii has a kink at $N = 82$ [16,26]. The slope of the linear dependence of r_c on the mass number suddenly changes at $N = 82$. Such behavior has been interpreted to be due to the stronger deformation away from the shell closure [26]. The charge radii obtained with the HF-SGII wave functions change linearly and their isotope dependence does not have a kink at $A = 138$. The charge radii calculated from the HF wave functions change more steeply than the observed ones for the isotopes with $A \leq 138$. It is theoretically interesting to investigate how this difference of behavior between experiment and HF calculations manifests itself in the asymmetries, although the measurement of asymmetries of the Ba isotopes is not easily accessible.

The charge radii as well as r_n, r_p, and Δr_{np} are shown in Table III for stable isotopes $A = 132 - 138$. r_c^m in Table III is defined by

$$r_c^m = r_c^{\rm exp}(A) + r_c({\rm SGII}, A = 138) - r_c^{\rm exp}(A = 138) \ . \tag{8}$$

The isotope dependence of r_c^m has the same slope as the experimental charge radii and agrees with r_c(SGII) at $A = 138$. The modified neutron and proton radii are defined by

$$r_n^m = r_n({\rm SGII}) r_c^m / r_c({\rm SGII}) \tag{9}$$

and

$$r_p^m = r_p({\rm SGII}) r_c^m / r_c({\rm SGII}) \ , \tag{10}$$

respectively, and $(\Delta r_{np}^m)^2 = (r_n^m)^2 - (r_p^m)^2$ and $(\Delta r'_{np})^2 = r_n^2 - (r_p^m)^2$. r_n^m and r_p^m now have kinks at $A = 138$.

The results for A_S obtained with the SGII-HF wave functions are shown by solid curves in Fig. 4. The dashed curves are obtained with the modified wave functions that reproduce r_n^m and r_p^m. In this case, the isotope dependences of both r_n and r_p are assumed to have kinks at $A = 138$, as does the experimental isotope dependence of r_c. Only proton radii are modified to r_p^m (neutron radii are kept to those of the SGII wave functions) in obtaining the dotted curves in Fig. 4. In this case, only the isotope dependence of r_p is assumed to have a kink. Though we cannot distinguish the solid and dashed curves, the difference between the dotted and other curves becomes apparent for isotopes with smaller mass numbers ($A = 132 - 134$) at low q ($0.4 \leq q \leq 0.7$ fm^{-1}).

TABLE III. The same as in Table I for Ba isotopes. r_c^m, r_n^m, and r_n^m are defined by Eqs. (8), (9), and (10), respectively. $(\Delta r_{np}^m)^2 = (r_n^m)^2 - (r_p^m)^2$ and $(\Delta r'_{np})^2 = r_n^2 - (r_p^m)^2$.

A	132	134	136	138
SGII				
r_c	4.813	4.824	4.834	4.845
r_n	4.840	4.867	4.892	4.916
r_p	4.764	4.777	4.790	4.802
Δr_{np}^2	0.730	0.868	0.988	1.108
$r_c^{\rm exp}$	4.825	4.826	4.828	4.832
r_c^m	4.838	4.840	4.841	4.845
r_n^m	4.865	4.883	4.899	4.916
r_p^m	4.789	4.793	4.797	4.802
$(\Delta r_{np}^m)^2$	0.734	0.871	0.989	1.108
$(\Delta r'_{np})^2$	0.491	0.715	0.920	1.108

We finally comment on the experimental feasibility in the case of Ba isotopes. The energy resolution required for the $A = 132$ isotope is about five times that required for ^{208}Pb. The magnitude of the cross section is reduced by $(56/82)^2$ compared to the case of Pb. As the change in Δr_{np} is as small as $\sim 0.5\%$ even in the case of $A = 132$, the machine time required to get this accuracy in Δr_{np} is

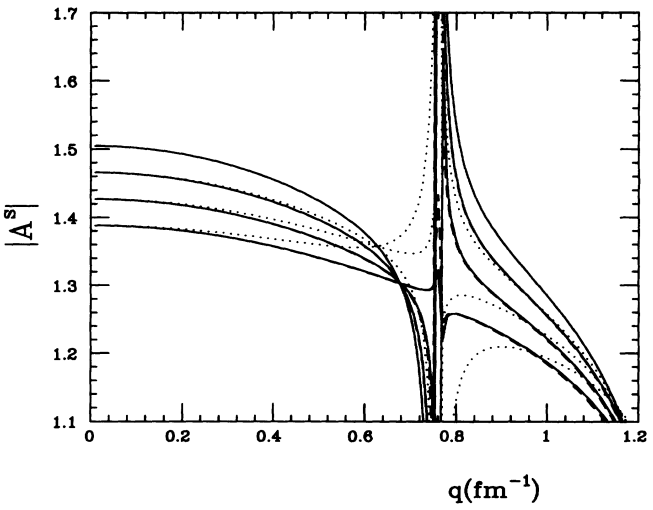

FIG. 4. The same as in Fig. 1 for Ba isotopes. The solid curve is the same as in Fig. 1. The dashed (dotted) curve is obtained by using the modified GSII-HF wave functions that reproduce the values of r_n^m and r_p^m (r_n and r_p^m) in Table III for neutron and proton radii, respectively.

about 20 times that for the case of ^{208}Pb. Unfortunately, the measurement of the asymmetries seems inaccessible for Ba isotopes at present.

One deficient point of the present method is that the target should be stable or at least have lifetime long enough to be able to carry out experiments. Ba isotopes become unstable in the region $A \leq 129$. There is a theoretical report that an interesting crossing between r_n and r_p is predicted around $A = 116$ in a relativistic mean-field calculation [27]. Unfortunately, we cannot investigate this point of the asymmetries of polarized electron scattering, as Ba isotopes are unstable in this extremely neutron-deficient mass region. The experimental study of the isotope dependence of Δr_{np} is, thus, restricted only to the region of stable isotopes.

III. SUMMARY

We studied the sensitivity of the asymmetries of longitudinally polarized elastic Coulomb electron scattering to the difference in radii of neutron and proton distributions in Ca, Sn, and Ba isotopes. Differences in the mass number dependence of Δr_{np} between HF calculations and observed values extracted from other experiments have been investigated for each kind of isotope. We can conclude that by looking at the asymmetries we can identify these differences for nuclei near ^{48}Ca in the case of Ca isotopes, for ^{116}Sn and ^{124}Sn in the case of Sn isotopes, and for ^{132}Ba in the case of Ba isotopes. The actual measurement of the asymmetries is accessible for Sn isotopes to detect Δr_{np} to the accuracy of 1–2 %, while it seems inaccessible for Ca and Ba isotopes in the present experimental situation. We believe that the measurement of the asymmetries can become another powerful tool to detect Δr_{np} in various nuclei in the near future with an improved experimental setup.

We add a comment on the case of Pb isotopes. The charge radii of Pb isotopes have an anomalous kink at $A = 208$. The observed charge radii of neutron-deficient isotopes ($A < 208$) follow the HF values rather well, while those of neutron-rich isotopes ($A > 208$) show deviations from the HF values [28]. The relativistic mean-field theory, on the other hand, can provide a good description of this anomalous kink at $A = 208$ [29]. Unfortunately, the stable Pb isotopes are on the lighter side of ^{208}Pb: $A = 202 - 208$. The study of the existence of such a kink at $A = 208$ in neutron and proton radii by investigating the isotopes on the heavier side is not accessible by polarized electron scattering for Pb isotopes. Nevertheless, the investigation of Δr_{np} for the isotopes with $A = 202 - 208$ is an interesting subject by itself and can provide information on neutron distributions in these nuclei. The measurement of the asymmetries is possible for the Pb isotopes in the present experimental situation.

Combined with analyses of (e, e) scattering experiments to get the proton radii of nuclei, one can use the asymmetries to deduce information on neutron radii of nuclei, as in the analyses of (p, p) scatterings from nuclei and atomic parity nonconservation (PNC) measurements [30]. We hope to get rich information on the mass number dependence of radii of neutron distributions in nuclei in various isotopes such as already obtained for charge radii. In spite of the restriction that the target should be stable in order to carry out experiments, the study of the asymmetries in polarized electron scattering can be a powerful method to investigate the isotope dependence of Δr_{np} to an accuracy higher than (or comparable to) other methods. The method of extracting neutron radii of nuclei from analyses of (p, p) scattering experiments as well as the atomic PNC measurements is also not free from this restriction.

ACKNOWLEDGMENTS

The author would like to express his thanks to Professor T. Otsuka for useful discussions. He also thanks Dr. W. Bentz for the careful reading of the manuscript. This work is supported in part by General Individual Research grant (B93-021) by Nihon University.

[1] J. Ashman *et al.*, Phys. Lett. B **206**, 364 (1988).
[2] D. B. Kaplan and A. Manohar, Nucl. Phys. **B310**, 527 (1988).
[3] L. A. Ahrens *et al.*, Phys. Rev. D **35**, 785 (1987).
[4] R. D. McKeown, Phys. Lett. B **219**, 140 (1989).
[5] D. H. Beck, Phys. Rev. D **39**, 3248 (1989).
[6] T. Suzuki, Nucl. Phys. **A515**, 609 (1990).
[7] T. Suzuki, Phys. Rev. C **45**, 1939 (1992).
[8] T. Suzuki, Y. Kohyama, and K. Yazaki, Phys. Lett. B **252**, 323 (1990).
[9] D. H. Beck, in *Proceedings of the Workshop on Parity Violation in Electron Scattering,* edited by E. J. Beise and R. D. McKeown (World Scientific, Singapore, 1990), p. 78.
[10] M. J. Musolf, T. W. Donnelly, J. Dubach, S. J. Pollock, S. Kowalski, and E. J. Beise, Phys. Rep. **239**, 1 (1994).
[11] T. Suzuki, J. Phys. G **19**, 1319 (1993).
[12] T. W. Donnelly, J. Dubach, and I. Sick, Nucl. Phys. **A503**, 589 (1989).
[13] J. L. Friar and J. W. Negele, Adv. Nucl. Phys. **8**, 219 (1975).
[14] S. Weinberg, Phys. Rev. Lett. **19**, 1264 (1967); A. Salam, in *Elementary Particle Physics,* edited by N. Svartholm (Almqvist and Wiksell, Stockholm, 1990), p. 367; S. L. Glashow, J. Iliopoulos, and L. Maiani, Phys. Rev. D **2**, 1285 (1970).
[15] U. Amaldi, A. Bohm, L. S. Durkin, P. Langacker, A. K. Mann, W. J. Marciano, A. Sirlin, and H. H. Williams, Phys. Rev. D **36**, 1385 (1987).
[16] A. Aufmuth, K. Heilig, and A. Steudel, At. Data Nucl. Data Tables **37**, 455 (1987).
[17] N. Van Giai and H. Sagawa, Phys. Lett. B **106**, 379

(1981).
[18] F. Tondeur, Phys. Lett. B **123** 139 (1983).
[19] S. Galster, H. Klein, J. Moritz, K. H. Schmidt, D. Wegener, and J. Bleckwenn, Nucl. Phys. **B32**, 221 (1971).
[20] W. R. Gibbs and J.-P. Dedonder, Phys. Rev. C **46**, 1825 (1992).
[21] M. J. Musolf and T. W. Donnelly, Nucl. Phys. **A546**, 509 (1992).
[22] R. L. Jaffe, Phys. Lett. B **229**, 275 (1989).
[23] C. J. Batty, E. Friedman, H. J. Gils, and H. Rebel, Adv. Nucl. Phys. **19**, 1 (1989).
[24] A. Kraznahorkay *et al.*, Phys. Rev. Lett. **66**, 1287 (1991).
[25] J. Friedrich and P.-G. Reinhard, Phys. Rev. C **33**, 335 (1986); J. Blocki and H. Flocard, Nucl. Phys. **A273**, 45 (1976); D. Vautherin, Phys. Rev. **7**, 296 (1973).
[26] A. C. Mueller *et al.*, Nucl. Phys. **A403**, 234 (1983).
[27] J. A. Sheikh, Phys. Rev. C **48**, 476 (1993).
[28] N. Tajima, P. Bonche, H. Flocard, P.-H. Heenen, and M. S. Weiss, Nucl. Phys. **A551**, 434 (1993).
[29] M. M. Sharma, G. A. Lalazissis, and P. Ring, Phys. Lett. B **317**, 9 (1993).
[30] S. J. Pollock, E. N. Fortson, and L. Wilets, Phys. Rev. C **46**, 2587 (1992).